

Magnetotransport properties of two-dimensional tellurium at high pressure

Huiyuan Guo(郭慧圆), Jialiang Jiang(姜家梁), Boyu Zou(邹博宇), Jie Cui(崔杰), Qinglin Wang(王庆林), Haiwa Zhang(张海娃), Guangyu Wang(王光宇), Guozhao Zhang(张国召), Kai Wang(王凯), Yinwei Li(李印威), and Cailong Liu(刘才龙)

Citation: Chin. Phys. B, 2025, 34 (**8**): 087301. DOI: 10.1088/1674-1056/add5c9
http://cpb.iphy.ac.cn; http://iopscience.iop.org/cpb

What follows is a list of articles you may be interested in

In-plane negative magnetoresistance and quantum oscillations in van der Waals antiferromagnet $DyTe_3$

Qi Qi(齐琦), Senhao Lv(吕森浩), Ke Zhu(祝轲), Yaofeng Xie(谢耀锋), Guojing Hu(胡国静), Zhen Zhao(赵振), Guoyu Xian(冼国裕), Yechao Han(韩烨超), Yang Yang(杨洋), Lihong Bao(鲍丽宏), Xiao Lin(林晓), Hui Guo(郭辉), Haitao Yang(杨海涛), and Hong-Jun Gao(高鸿钧)

Chin. Phys. B, 2025, 34 (**7**): 077305. DOI: 10.1088/1674-1056/adcc87

Nonvolatile ferroelectric control of electronic properties of Bi_2Te_3

Xusheng Ding(丁旭升), Yunfei Li(李云飞), Chaoyang Kang(康朝阳), Ye-Heng Song(宋业恒), and Weifeng Zhang(张伟风)

Chin. Phys. B, 2024, 33 (**11**): 117301. DOI: 10.1088/1674-1056/ad7670

Magnetic and electrical transport properties in GdAlSi and SmAlGe

Jing Gong(巩静), Huan Wang(王欢), Xiao-Ping Ma(马小平), Xiang-Yu Zeng(曾祥雨), Jun-Fa Lin(林浚发), Kun Han(韩坤), Yi-Ting Wang(王乙婷), and Tian-Long Xia(夏天龙)

Chin. Phys. B, 2024, 33 (**7**): 077302. DOI: 10.1088/1674-1056/ad41ba

Nonmonotonic anomalous Hall effect and anisotropic magnetoresistance in $SrRuO_3/PbZr_{0.52}Ti_{0.48}O_3$ heterostructures

Zhen-Li Wang(王振礼), Chao-Yang Kang(康朝阳), Cai-Hong Jia(贾彩虹), Hai-Zhong Guo(郭海中), and Wei-Feng Zhang(张伟风)

Chin. Phys. B, 2023, 32 (**10**): 107303. DOI: 10.1088/1674-1056/accd58

Nonlinear current response and electric quantum oscillations in the Dirac semimetal Cd_3As_2

Hao-Nan Cui(崔浩楠), Ze-Nan Wu(吴泽南), Jian-Kun Wang(王建坤), Guang-Yu Zhu(祝光宇), Jia-Jie Yang(杨佳洁), Wen-Zhuang Zheng(郑文壮), Zhi-Min Liao(廖志敏), Shuo Wang(王硕), Ben-Chuan Lin(林本川), and Dapeng Yu(俞大鹏)

Chin. Phys. B, 2023, 32 (**8**): 087306. DOI: 10.1088/1674-1056/acd9c5

SPECIAL TOPIC — Structures and properties of materials under high pressure

Magnetotransport properties of two-dimensional tellurium at high pressure

Huiyuan Guo(郭慧圆)[1], Jialiang Jiang(姜家梁)[1], Boyu Zou(邹博宇)[1], Jie Cui(崔杰)[1], Qinglin Wang(王庆林)[1,†], Haiwa Zhang(张海娃)[1], Guangyu Wang(王光宇)[1], Guozhao Zhang(张国召)[1], Kai Wang(王凯)[1], Yinwei Li(李印威)[2], and Cailong Liu(刘才龙)[1,‡]

[1] *School of Physics Science & Information Technology, Key Laboratory of Quantum Materials Under Extreme Conditions in Shandong Province, Liaocheng University, Liaocheng* 252059, *China*

[2] *Laboratory of Quantum Functional Materials Design and Application, School of Physics and Electronic Engineering, Jiangsu Normal University, Xuzhou* 221116, *China*

(Received 25 February 2025; revised manuscript received 23 April 2025; accepted manuscript online 8 May 2025)

Two-dimensional tellurium (2D-Te) exhibits strong spin–orbit coupling and a chiral structure. Studying its magnetotransport properties is crucial for the development of spintronic technologies and the exploration of novel device applications. The magnetotransport properties of 2D-Te under varying temperatures and high pressures warrant further study. In this paper, the magnetotransport behavior of 2D-Te under low-temperature and high-pressure conditions is investigated. At room temperature, the magnetoresistance (MR) increases with increasing magnetic field, exhibiting positive MR behavior below 4.3 GPa. During decompression, MR is almost constant with decreasing pressure. MR is more sensitive to pressure at lower temperatures.

Keywords: magnetoresistance, 2D-Te, high pressure, low temperature

PACS: 73.43.Qt, 75.47.–m, 81.40.Vw

DOI: 10.1088/1674-1056/add5c9 **CSTR:** 32038.14.CPB.add5c9

1. Introduction

Since the initial discovery of monolayer graphene in 2004, various two-dimensional (2D) materials, such as tellurium, transition metal dichalcogenides and black phosphorus have attracted considerable attention.[1–5] With their high specific surface area,[6] high carrier mobility[7] and excellent thermoelectric properties,[8] 2D materials hold significant promise for applications in energy storage,[9] luminescence[10] and catalysis.[11,12] 2D materials also demonstrate considerable potential for applications in spintronics. For instance, graphene nanoribbons with a "zigzag" edge shape exhibited an electronic bandgap of roughly 0.2–0.3 eV, and the magnetic order on the graphene edges remained stable even at room temperature.[13] Bulk VSe_2 behaved paramagnetically, but in the monolayer state, it exhibited a significant ferromagnetic order that persisted above room temperature.[14] The interlayer magnetism of 2D $CrBr_3$ was stacking-dependent: a single layer of $CrBr_3$ was ferromagnetic, whereas the interlayer coupling in bilayers depended on the stacking sequence and could be either ferromagnetic or antiferromagnetic.[15]

Two-dimensional tellurium (2D-Te) exhibits strong spin–orbit coupling and has a chiral structure.[16–19] Recently, several breakthroughs have been made in the study of 2D-Te magnetism. For instance, Zhang *et al.* studied the longitudinal and transverse magnetoresistance (MR) of tellurium flakes at low temperatures, revealing that the longitudinal negative MR persisted at temperatures up to 200 K, while longitudinal magnetoconductivity transitioned from parabolic to linear field dependence with decreasing temperature. These findings extend the application of Weyl physics and shed light on the design of topological semiconductor devices.[20] Niu *et al.* revealed a pressure-induced insulator-to-metal transition, two-carrier transport and a non-trivial π Berry phase shift in quantum oscillations in 2D-Te.[21] Therefore, the study of magnetotransport behavior of 2D-Te under low temperatures and high pressures is crucial for the design of next-generation spintronic devices.

In this work, the transverse MR of 2D-Te was studied at low temperatures and high pressures. At room temperature, MR increases with increasing magnetic field, exhibiting a positive MR behavior below 4.3 GPa. During decompression, MR remains almost constant with decreasing pressure. MR is more sensitive to pressure at lower temperatures.

2. Experimental methods

The 2D-Te was synthesized using a physical vapor deposition method in conjunction with a horizontal vacuum tube furnace. The high pressure was applied using a diamond anvil cell (DAC) with anvil culet of 400 μm diameter. A nonmag-

†Corresponding author. E-mail: wangqinglin@lcu.edu.cn

‡Corresponding author. E-mail: cailong_liu@lcu.edu.cn

© 2025 Chinese Physical Society and IOP Publishing Ltd. All rights, including for text and data mining, AI training, and similar technologies, are reserved.

netic rhenium sheet, approximately 50 μm thick, was used as the gasket, and a 355 nm laser was employed to fabricate holes with diameters of 200 μm. Cubic boron nitride (c-BN) was mixed with an epoxy resin binder and then pressed into the holes to serve as an insulating layer. A sample chamber with a diameter of 120 μm was then fabricated at the center of the indentation. NaCl powder was loaded into the sample chamber as a pressure-transmitting medium. A 2D-Te flake with around 50 nm thickness and a ruby ball with a diameter of < 10 μm were loaded into the sample chamber. The loaded DAC was then enclosed within a closed-cycle cryostat to achieve low-temperature and high-pressure conditions, and MR was measured using a transport measurement system (ET9110-HS, East Changing Technologies, China).[22]

3. Results and discussion

According to Boltzmann's transport theory, MR results from the Lorentz force deflecting the electron trajectory and is directly related to electron scattering paths close to the Fermi surface[23] MR is defined as[24–27]

$$\mathrm{MR} = [R(B) - R(0)]/R(0) \times 100\%. \tag{1}$$

To minimize experimental errors, MR has been symmetrized:

$$\mathrm{MR} = (\mathrm{MR}_1 + \mathrm{MR}_2)/2, \tag{2}$$

where MR_1 and MR_2 denote the data measured under a negative magnetic field and a positive magnetic field, respectively. Figure 1 shows the relationship between MR and magnetic field with increasing pressure at room temperature. Below 4.3 GPa, MR shows a symmetric, parabolic-like behavior with the magnetic field, which exhibits positive MR behavior. This behavior was attributed to the low-dimensional confinement, enhancing the inter-electron interactions.[28] No MR saturation is observed in the studied magnetic field range. In the pressure range of 4.3–11.1 GPa, MR behavior almost disappears.

The pressure dependence of MR at room temperature under a magnetic field of 1.2 T is shown in Fig. 2. MR exhibits discontinuities at 0.9 GPa, 3.4 GPa, 4.3 GPa and 7.6 GPa, respectively. Phase transitions in 2D-Te are strongly correlated with a change of MR trends. The change at 0.9 GPa was ascribed to the Lifshitz transition, caused by the unique camelback-shaped dispersion of the valence band in Te.[29] The Lifshitz transition is characterized by changes in the topological structure of the Fermi surface, while carrier mobility is closely related to the density of states and band structure near the Fermi level. Our previous study demonstrated that the discontinuity in the μ–P curve at 0.9 GPa is indicative of a Lifshitz transition in 2D-Te.[22] The Fermi level of Te crossed the lowest energy point (E_c) located near the H point, resulting in a distortion of the energy band structures and leading to the Lifshitz transition. The discontinuous change in MR at 3.4 GPa was attributed to a phase transition from a semiconductor to a Weyl semimetal.[29] The discontinuous change in MR at 4.3 GPa was associated with the structural transition from Te-I to Te-II, whereas the discontinuous change at 7.6 GPa was related to the transition from Te-II to Te-III.[30–32]

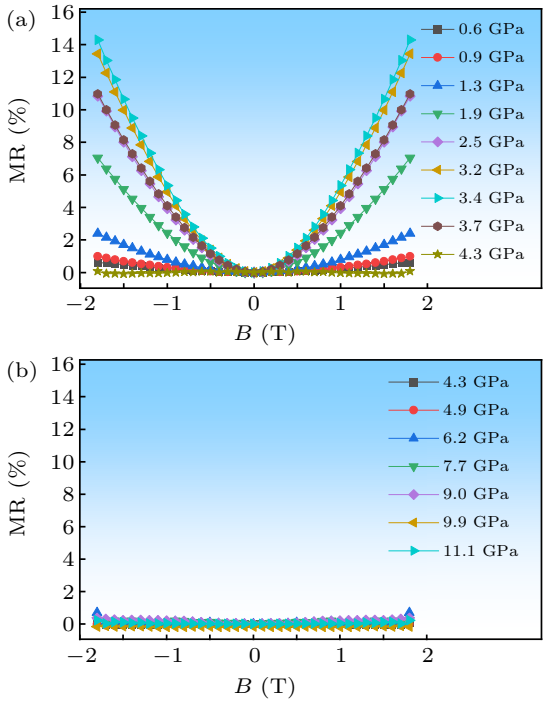


Fig. 1. Magnetic field dependence of MR at room temperature and different pressures.

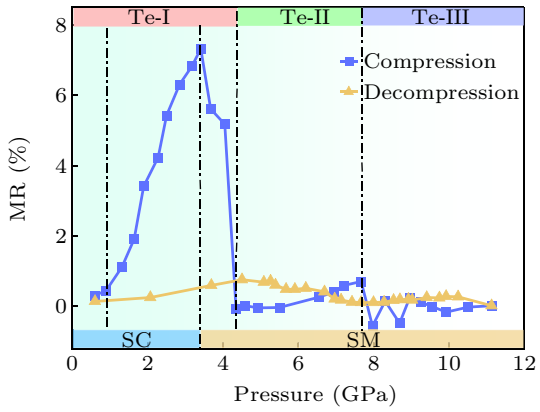


Fig. 2. The pressure dependence of MR at room temperature and 1.2 T. SC and SM represent semiconductor and semimetal, respectively.

Generally, MR undergoes abrupt changes during the transition from semiconductor to semimetal.[33,34] According to the electronic conduction model and the pressure-induced impurity ionization model, the atoms deviate from their equilibrium positions and introduce additional energy levels (strain-induced impurity energy levels) in the bandgap with increasing pressure. Below 3.4 GPa, the carrier conduction in 2D-Te was primarily governed by carriers excited both over the whole bandgap and from strain-induced impurity energy levels.[35,36] With pressure increasing, the ionization of carriers from impurity levels combined with bandgap narrowing led to an increase in carrier concentration. This, in turn, enhanced the

sensitivity of spin-dependent scattering and electron–phonon scattering to the external magnetic field, thereby increasing MR. In the Weyl semimetal state, the valence and conduction bands eventually overlap with increasing pressure, leading to an increase in electron concentration. Consequently, the dominant carriers transition from holes to electrons and holes, resulting in carrier recombination and a reduction in the effective carrier concentration. This weakens spin-dependent scattering, thereby leading to a decrease in MR.[22,29,37] It is worth mentioning that MR almost disappears above 4.3 GPa, as the comparable concentrations of electrons and holes reduce the effective carrier concentration and weaken spin-dependent scattering.[22] During decompression, the pressure-induced suppression of MR is irreversible. Our previous Raman studies showed that the pressure-induced phase transitions in 2D-Te were reversible.[22] Therefore, the irreversible MR was not due to phase transitions but rather stemmed from the non-recovery of the effective carrier concentration.

The MR results measured at low temperature and high pressure are shown in Fig. 3. Positive MR behavior is observed, similar to that at room temperature. The pressure dependence of MR at 1.2 T and different temperatures is shown in Fig. 4(a). The mean free path increased with decreasing temperature, leading to weakened spin-dependent scattering and a reduction in zero-field resistance, $R(0)$.[38] According to the pressure dependence of resistivity at different temperatures (Fig. 4(b)), $R(B)$ remains almost constant with temperature. Therefore, MR is more sensitive to pressure at lower temperatures.

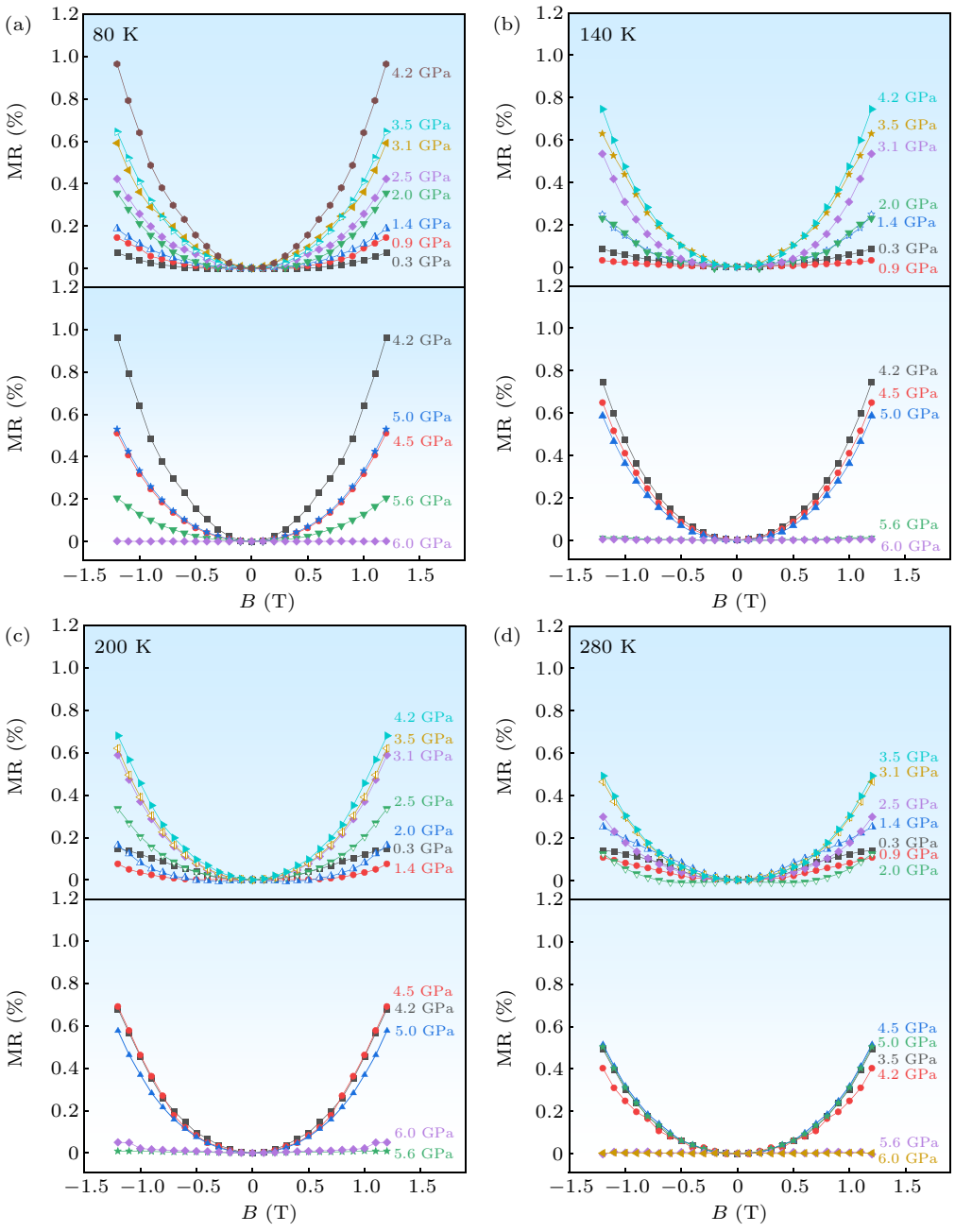


Fig. 3. Magnetic field dependence of MR at (a) 80 K, (b) 140 K, (c) 200 K and (d) 280 K under different pressures.

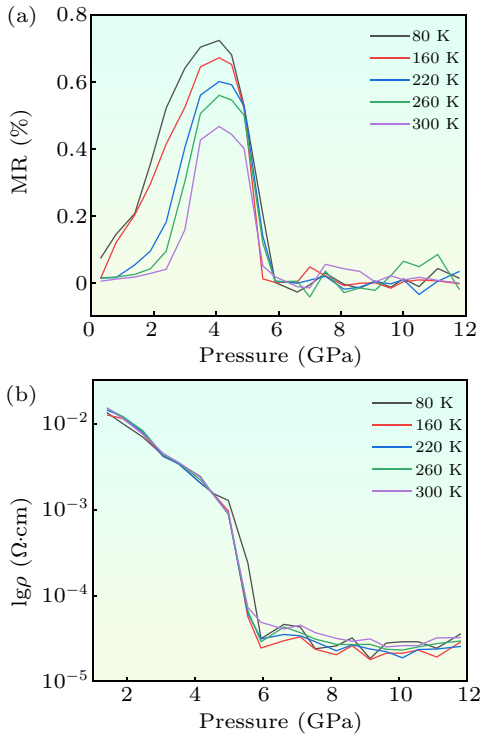


Fig. 4. The pressure dependence of (a) MR and (b) resistivity (ρ) at selected temperatures and 1.2 T.

4. Conclusion

The magnetotransport properties of 2D-Te were studied under low temperature and high pressure. At room temperature, MR exhibits positive MR behavior below 4.3 GPa. During decompression, MR is almost constant with decreasing pressure. Moreover, MR is more sensitive to pressure at lower temperatures. This work enriches the understanding of the magnetotransport behavior of 2D-Te under temperature–pressure conditions, which provides guidance for the design of novel spintronic devices.

Acknowledgments

Project supported by the National Key R&D Program of China (Grant No. 2023YFA1406200), the National Natural Science Foundation of China (Grant No. 12304067), the Natural Science Foundation of Shandong Province (Grant Nos. ZR2021QA087 and ZR2021QA092), and the Special Construction Project Fund for Shandong Province Taishan Scholars.

References

[1] Novoselov K S, Geim A K, Morozov S V, Jiang D, Zhang Y, Dubonos S V, Grigorieva I V and Firsov A A 2004 *Science* **306** 666
[2] Mi M J, Xiao H, Yu L X, Zhang Y X, Wang Y S, Cao Q and Wang Y L 2023 *Mater. Today Nano* **24** 100408
[3] Zhang H M, Song D Z, Huang F Y, Zhang J and Jiang Y P 2023 *Chin. Phys. B* **32** 066802
[4] Yu W T, Zhao L, Gao Y F, Gao S P, Yang Y K, Pan C, Liang S J and Cheng B 2025 *Chin. Phys. B* **34** 018502
[5] Pan Y H, Lei B, Qiao J S, Hu Z X, Zhou W and Ji W 2020 *Chin. Phys. B* **29** 086801
[6] Luo J, Qiao R and Ding B F 2024 *Matter* **7** 3351
[7] Khazaei M, Arai M, Sasaki T, Estili M and Sakka Y 2014 *Phys. Chem. Chem. Phys.* **16** 7841
[8] Anh D T K, Minh P H, Yamanoi K, Cadatal-Raduban M, Mui L V, Hieu D M and Hung N D 2024 *Appl. Sci.* **14** 9257
[9] Xue Y H, Zhang Q, Wang W J, Cao H, Yang Q H and Fu L 2017 *Adv. Energy Mater.* **7** 1602684
[10] Zhong F, Nie G Z, Lang Y F, Zhang Z W, Li H L, Gan L F, Xu Y and Zhao Y Q 2023 *Phys. Chem. Chem. Phys.* **25** 3175
[11] Huang G W, Liu H, Wang S P, Yang X, Liu B H, Chen H Z and Xu M S 2015 *J. Mater. Chem. A* **3** 24128
[12] Lukowski M A, Daniel A S, English C R, Meng F, Forticaux A, Hamers R J and Jin S 2014 *Energy Environ. Sci.* **7** 2608
[13] Magda G Z, Jin X Z, Hagymási I, Vancsó P, Osváth Z, Nemes-Incze P, Hwang C, Biró L P and Tapasztó L 2014 *Nature* **514** 608
[14] Bonilla M, Kolekar S, Ma Y J, Diaz H C, Kalappattil V, Das R, Eggers T, Gutierrez H R, Phan M H and Batzill M 2018 *Nat. Nanotechnol.* **13** 289
[15] Chen W J, Sun Z Y, Wang Z J, Gu L H, Xu X D, Wu S W and Gao C L 2019 *Science* **366** 983
[16] Calavalle F, Suárez-Rodríguez M, Martín-García B, Johansson A, Vaz D C, Yang H Z, Maznichenko I V, Ostanin S, Mateo-Alonso A, Chuvilin A, Mertig I, Gobbi M, Casanova F and Hueso L E 2022 *Nat. Mater.* **21** 526
[17] Dong Z Y and Ma Y H 2020 *Nat. Commun.* **11** 1588
[18] Ben-Moshe A, Da Silva A, Müller A, Abu-Odeh A, Harrison P, Waelder J, Niroui F, Ophus C, Minor A M, Asta M, Theis W, Ercius P and Alivisatos A P 2021 *Science* **372** 729
[19] Wang Y, Lei Z Z, Zhang J S, Tao X Y, Hua C Q and Lu Y H 2023 *Chin. Phys. Lett.* **40** 117102
[20] Zhang N, Cheng B, Li H, Li L and Zeng C G 2021 *Chin. Phys. B* **30** 087304
[21] Niu C, Zhang Z C, Graf D, Lee S, Wang M Y, Wu W Z, Low T and Ye P D 2023 *Commun. Phys.* **6** 345
[22] Zou B Y, Wang S, Wang Q L, Wang G Y, Zhang G Z, Jiang J L, Cui J, He J R, Xi H Z, Fu H L, Wang Z C, Wang C, Wang Q S and Liu C L 2024 *Appl. Phys. Lett.* **124** 102105
[23] Li X, Sun J P, Shahi P, Gao M, MacDonald A H, Uwatoko Y, Xiang T, Goodenough J B, Cheng J G and Zhou J S 2018 *Proc. Natl. Acad. Sci. USA* **115** 9935
[24] Ali M N, Schoop L M, Garg C, Lippmann J M, Lara E, Lotsch B and Parkin S S P 2016 *Sci. Adv.* **2** e1601742
[25] Li T, Wang S Y, Chen X L, Chen C H, Fang Y and Yang Z R 2024 *Chin. Phys. B* **33** 066401
[26] Gong J, Wang H, Ma X P, Zeng X Y, Lin J F, Han K, Wang Y T and Xia T L 2024 *Chin. Phys. B* **33** 077302
[27] Zhang N, Zhao G, Li L, Wang P D, Xie L, Cheng B, Li H, Lin Z Y, Xi C Y, Ke J Z, Yang M, He J Q, Sun Z, Wang Z F, Zhang Z Y and Zeng C G 2020 *Proc. Natl. Acad. Sci. USA* **117** 11337
[28] Lee P A and Ramakrishnan T V 1985 *Rev. Mod. Phys.* **57** 287
[29] Ideue T, Hirayama M, Taiko H, Takahashi T, Murase M, Miyake T, Murakami S, Sasagawa T and Iwasa Y 2019 *Proc. Natl. Acad. Sci. USA* **116** 25530
[30] Li X, Huang X L, Wang X, Liu M K, Wu G, Huang Y P, He X, Li F F, Zhou Q, Liu B B and Cui T 2018 *Phys. Chem. Chem. Phys.* **20** 6116
[31] Parthasarathy G and Holzapfel W B 1988 *Phys. Rev. B* **37** 8499
[32] Ohmasa Y, Yamamoto I, Yao M and Endo H 1995 *J. Phys. Soc. Jpn.* **64** 4766
[33] Wang J, Wang S Y, He X Y, Zhou Y, An C, Zhang M, Zhou Y H, Han Y Y, Chen X L, Zhou J and Yang Z R 2022 *Phys. Rev. B* **106** 045106
[34] Zhang J L, Jin L, Chen J, Zhang C H, Li P, Yuan Y, Wen Y, Zhang Q, Zhang X M, Liu E K, Wang W H and Zhang X X 2021 *New J. Phys.* **23** 083041
[35] Yao M G, Wåberg T and Sundqvist B 2010 *Phys. Rev. B* **81** 155441
[36] Liu B, Yang J, Han Y H, Hu T J, Ren W B, Liu C L, Ma Y Z and Gao C X 2011 *J. Appl. Phys.* **109** 053717
[37] Ohashi M, Oomi G, Ohmichi E, Osada T, Takano K, Sakurai H and Itoh F 2008 *J. Appl. Phys.* **104** 073901
[38] Van Gorkom R P, Caro J, Klapwijk T M and Radelaar S 2001 *Phys. Rev. B* **63** 134432